CHIN. PHYS. LETT. Vol. 38, No. 1 (2021) 013401

Rabi Oscillations and Coherence Dynamics in Terahertz Streaking-Assisted Photoelectron Spectrum

Shuai Wang(王帅)[1,4], Zhiyuan Zhu(朱志远)[1,2,4*], Yizhu Zhang(张逸竹)[3], Tian-Min Yan(阎天民)[2*], and Yuhai Jiang(江玉海)[1,2,5*]

[1]*School of Physical Science and Technology, ShanghaiTech University, Shanghai 201210, China*
[2]*Shanghai Advanced Research Institute, Chinese Academy of Sciences, Shanghai 201210, China*
[3]*Center for Terahertz Waves and College of Precision Instrument and Optoelectronics Engineering, Key Laboratory of Opto-electronics Information and Technical Science (Ministry of Education), Tianjin University, Tianjin 300072, China*
[4]*Shanghai Institute of Applied Physics, Chinese Academy of Sciences, Shanghai 201204, China*
[5]*University of Chinese Academy of Sciences, Beijing 100049, China*

(Received 13 September 2020; accepted 24 November 2020; published online 6 January 2021)

We present an approach, a Terahertz streaking-assisted photoelectron spectrum (THz SAPS), to achieve direct observations of ultrafast coherence dynamics with timescales beyond the pulse duration. Using a 24 fs probe pulse, the THz SAPS enables us to well visualize Rabi oscillations of 11.76 fs and quantum beats of 2.62 fs between the $5S_{1/2}$ and $5P_{3/2}$ in rubidium atoms. The numerical results show that the THz SAPS can simultaneously achieve high resolution in both frequency and time domains without the limitation of Heisenberg uncertainty of the probe pulse. The long probe pulse promises sufficiently high frequency resolution in photoelectron spectroscopy allowing to observe Autler–Townes splittings, whereas the streaking THz field enhances temporal resolution for not only Rabi oscillations but also quantum beats between the ground and excited states. The THz SAPS demonstrates a potential applicability for observation and manipulation of ultrafast coherence processes in frequency and time domains.

DOI: 10.1088/0256-307X/38/1/013401

The advent of ultrashort pulse technique enables us to directly observe ultrafast processes in atoms and molecules, providing insight into ultrafast dynamics up to picoseconds. One of the most common techniques is known as the pump-probe approach, where the pulsed laser is used to initiate the reactions by launching wavefunction to excited states. The probe pulse is then used to interrogate reactions at various time delays. Finally, the time evolution of reactions can be traced as a function of the pump-probe delay time. With the developments of the ultrafast technique in recent years, the observation and steering of electronic dynamics at the time scale in a few of femtoseconds even up to attoseconds have attracted considerable interests both theoretically and experimentally.[1–6] For instance, many amazing ultrafast phenomena such as the coherence population transfer between discrete energy levels,[7] real-time observation of valence electron motion,[8] and the breakage of chemical bonds[9] were investigated in the atomic and molecular scales and in femtosecond timescales, where the temporal duration of laser pulses is required to be shorter than the dynamic processes.

The Rabi oscillation is the population cycle between two levels in a quantum system in the presence of an oscillatory driving field.[10] In the frequency domain, Autler–Townes splitting (ATS), known as an AC Stark effect proposed by Autler and Town,[11] was employed to control and to detune ultrafast population transfer in Rabi oscillation. Efficient population transfer in the Rabi process on a short time scale is the foundation of quantum information processing.[12] The dynamical controlling light absorption with ATS allows for highly efficient broadband and long-life quantum information storage.[13]

The ATS dynamics in real time can be observed with time-resolved photoelectron spectroscopy, which contains various information about ionization process. Controlling and observing the correlated electron dynamics for ATS were reported[14] in photoelectron spectrum in the nonperturbative strong ionization regime. ATS in the multiphoton resonance ionization spectrum with ultrashort laser pulses has also been proposed in molecules.[15] More recently, two-photon Rabi oscillations between the $1s2p$ and $1s6f$ Rydberg states have been observed with photoelectron spectra, and proved on the timescales as short as tens of femtoseconds in helium.[16] Such a short timescale is sufficient to implement the coherence control against the decay of coherence. Thus, attosecond pulse, whose duration is shorter than the time scale of dynamics, is imperative to observe the ultrafast dynamics. However, a tabletop-scale sub-femtosecond metrology is not easy to realize. It brings up the problem whether or not the temporal information can be measured with relatively long pulses.

For those measurements, the laser-field-driven

Supported by the National Natural Science Foundation of China (Grant Nos. 11827806, 11874368 and 61675213).
*Corresponding authors. Email: zhuzhy@shanghaitech.edu.cn; yantm@sari.ac.cn; jiangyh@sari.ac.cn
© 2021 Chinese Physical Society and IOP Publishing Ltd

streaking scheme can access electron dynamics or pulse diagnostic of temporal profile in the accuracy of subfemtosecond and even attosecond.[17–20] One of showcases is the temporal characterization of x-ray pulses with sub-femtosecond resolution.[21] The streaking photoelectrons have been used to monitor nonadiabatic dynamics in the vicinity of conical intersections and to provide direct signatures of electronic coherences in high temporal resolution.[22] As the probe laser, the terahertz(THz)-streaking method has already been employed to measure Coulomb-laser coupling-induced time shifts in photoionization.[23] Recently, we extended THz-streaking methods to a time-resolved THz streaking-assisted photoelectron spectrum (THz SAPS), where the THz pulse is exploited as an assisted field and synchronized with a femtosecond XUV pulse.[24] In THz SAPS, the center of THz field is locked to the center of the XUV pulse, to steer the electron trajectory and to effectively broaden the momentum distribution of photoelectron. With the broadened spectral peaks, the yielding interference patterns allow one to reconstruct the relative phase between the associated states and extract the information of quantum coherence, which could not be accessed merely from intensity-encoded spectral peaks. Time-evolved density matrix elements can be reconstructed from the streaking-assisted photoelectron spectrum. Simultaneously, the coherence dynamics can be mapped on the photoelectron spectra and temporally resolved beyond the pulse duration.

In this Letter, we propose an approach of Terahertz streaking-assisted photoelectron spectrum (THz SAPS) to study Rabi oscillation (11.76 fs) and coherence dynamic (2.62 fs) of $5S_{1/2}$ and $5P_{3/2}$ in the rubidium atom, where the probe pulse of 24 fs in full-width at half maximum (FWHM) combining with a 5.3 THz field is utilized. The use of long ultraviolet (UV, 266 nm) probe pulse allows to directly observe Autler–Townes splittings without the THz-assisted field in the photoelectron spectrum. As THz field amplitude rises, both Rabi oscillation and ultrafast coherence between the ground state and the excited state are visible in THz SAPS with sufficiently enhanced temporal resolution.

In the THz SAPS method, the atom is subject to linearly polarized fields and the photoelectron ionization signal $w(p;\tau)$ collected along the polarization direction can be analyzed under the strong field approximation (SFA). The dynamics of the system at any time τ are mapped directly onto $w(p;\tau) = |p||M_{\rm p}|^2$, with different elements of density matrix differentiated by longitudinal momentum p. Here τ is time delay between the probe pulse and the pump pulse. The amplitude of the direct ionization in the length gauge under the SFA reads

$$M_{\rm p} = \lim_{t\to\infty}\int^{t} dt' e^{iS_{\rm p}(t')}\langle p + A(t')|\hat{\mu}E(t')|\Psi_0(t')\rangle, \quad (1)$$

where $S_{\rm p}(t') = \frac{1}{2}\int^{t'} dt''[p + A(t'')]^2$, and $A(t')$ is the vector potential. The initial state $|\Psi_0(t')\rangle$ can be prepared as the superposition of states $|\psi_i\rangle$ with the ionization energy $I_{\rm p}^{(i)}$, $|\Psi_0(t')\rangle = \sum_i c_i(t')e^{{\rm i}I_{\rm p}^{(i)}t'}|\psi_i\rangle$. In linearly polarized fields, $E(t') = E_{\rm UV}(t') + E_{\rm THz}(t')$ and $A(t') = A_{\rm UV}(t') + A_{\rm THz}(t')$. Because the duration of the UV field pulse is much smaller than the THz field, the latter is approximately linear, $A_{\rm THz} \cong \alpha t'$, where $\alpha = -E_0^{\rm THz}$. The distribution $|M_{\rm p}(\tau)|^2$ comprises Gaussian peaks for all population and coherence terms, $|M_{\rm p}(\tau)|^2 = \left(\frac{\pi[E_0^{\rm (UV)}]^2}{2|b(p)|}\right)[W_{\rm pop}(p;\tau) + W_{\rm coh}(p;\tau)]$ (see Ref. [24]), with

$$W_{\rm pop}(p;\tau) = \sum_i \rho_{ii}(\tau)e^{-\frac{[\bar{\Omega}_{ii}(p)]^2}{|b(p)\sigma|^2}}, \quad (2)$$

$$W_{\rm coh}(p;\tau) = 2\sum_{i,j<i}{\rm Re}\left[\rho_{ij}(\tau)e^{i\frac{\alpha p\bar{\Omega}_{ij}(p)\Delta_{ij}}{|b(p)|^2}}\right] \cdot e^{-\frac{[\bar{\Omega}_{ij}(p)]^2}{|b(p)\sigma|^2}}e^{-\frac{(\Delta_{ij}/2)^2}{|b(p)\sigma|^2}}, \quad (3)$$

from which the positions and widths of spectral peaks are easily seen. Here, $\bar{\Omega}_{ii}(p) = \frac{p^2}{2} + I_{\rm p}^{(i)} - \omega_{\rm UV}$, $\bar{\Omega}_{ij}(p) = \frac{p^2}{2} + \frac{I_{\rm p}^{(i)}+I_{\rm p}^{(j)}}{2} - \omega_{\rm UV}$, $\Delta_{ij} = I_{\rm p}^{(i)} - I_{\rm p}^{(j)}$, and ρ_{ij} are density matrix elements, including the population ρ_{ii} and the coherence $\rho_{ij}(i \neq j)$, where $\omega_{\rm UV}$ is the photon energy of UV field and $I_{\rm p}^{(i)}$ is the ionization potential of the ith state. Spectral peaks appear at p with $\bar{\Omega}_{ii}(p) = 0$. The widths of peaks on photoelectron spectra are determined by

$$|b(p)\sigma| = \sqrt{1/\sigma^2 + (\alpha p\sigma)^2} \quad (4)$$

with $b(p) = 1/\sigma^2 - i\alpha p$, which depends on the THz field amplitude α and the UV-field temporal width σ (standard deviation). In Eq. (3), usually $W_{\rm coh}$ is much smaller than $W_{\rm pop}$ due to the presence of the last exponential term of $\Delta_{ij} = I_{\rm p}^{(i)} - I_{\rm p}^{(j)}$. However, when the THz field increases, the relative amplitude of $W_{\rm coh}$ enhances and quantum coherent fringes will appear, where coherence dynamics can be displayed on photoelectron spectra. The period of fringes for quantum coherence is determined by the real part of $W_{\rm coh}(p;\tau)$ in Eq. (3), i.e.,

$$\begin{aligned}&{\rm Re}[W_{\rm coh}(p;\tau)]\\ &= |\rho_{ij}(\tau)|\cos\left[-\Delta_{ij}\tau + \frac{\Delta_{ij}\alpha p_{ij}^2(p-p_{ij})}{\frac{1}{\sigma^4} + \alpha^2 p_{ij}^2}\right].\end{aligned} \quad (5)$$

The period of fringe is determined by $-\Delta_{ij}$.

Now, we study Rabi oscillation and ATS. Using the time-resolved THz SAPS method, we present the momentum distribution for a system of H_0 undergoing Rabi oscillation driven by an external light field $H' = -\mu E(e^{-i\omega t} + e^{i\omega t})$, where $\hat{\mu}$ is the transition dipole, E and ω are electronic field and frequency of the external electric field, respectively. The evolution of such a system is governed by the Schrödinger equation

$$i\hbar\frac{\partial}{\partial t}\Psi = (H_0 + H')\Psi. \quad (6)$$

Equation (6) can be solved using the perturbation method. The amplitudes are given by

$$c_{\rm g}(t) = \sqrt{\frac{1}{2}}e^{-\frac{i\Omega t}{2}} + \sqrt{\frac{1}{2}}e^{\frac{i\Omega t}{2}}, \tag{7}$$

$$c_{\rm e}(t) = -\sqrt{\frac{1}{2}}e^{-\frac{i\Omega t}{2}} + \sqrt{\frac{1}{2}}e^{\frac{i\Omega t}{2}}, \tag{8}$$

where subscripts g and e stand for the ground state and the first excited state, respectively. $\Omega = \frac{2\mu_{10}E}{\hbar}$ is the so-called Rabi frequency.

In order to study the photoelectron spectrum in the dressed system, Eqs. (7) and (8) can be substituted into $|\Psi_0(t')\rangle$. The energy level of E_i [equals $-I_{\rm p}^{(i)}$] splits into $E_i \pm \frac{\Omega}{2}$ (i = e or g for the excited state or the ground state), as shown in Fig. 1(a). We assume that $|i+\rangle$ and $|i-\rangle$ are the split states, whose energy levels are $E_{i+} = E_i + \frac{\Omega}{2}$ and $E_{i-} = E_i - \frac{\Omega}{2}$. $\bar{\Omega}_{ii}(p)$ in Eq. (2) turns to $\bar{\Omega}_{ii}^{+}(p) = \frac{p^2}{2} + I_{\rm p}^{(i)} - \omega_{\rm UV} - \frac{\Omega}{2}$ and $\bar{\Omega}_{ii}^{-}(p) = \frac{p^2}{2} + I_{\rm p}^{(i)} - \omega_{\rm UV} + \frac{\Omega}{2}$. Then Eq. (2) can be written as

$$W_{\rm pop}(p;\tau) = \sum_{i={\rm e(g)}} \rho_{ii}(\tau)\left(e^{-\frac{[\bar{\Omega}_{ii}^{+}(p)]^2}{|b(p)\sigma|^2}} + e^{-\frac{[\bar{\Omega}_{ii}^{-}(p)]^2}{|b(p)\sigma|^2}}\right) \tag{9}$$

and $W_{\rm coh}(p;\tau)$ is the same as Eq. (3). Spectral peaks appear at $\bar{\Omega}_{ii}^{+}(p) = 0$ and $\bar{\Omega}_{ii}^{-}(p) = 0$, respectively, whose solutions include $p_{ii} = \sqrt{2[\pm\frac{\Omega}{2} - I_{\rm p}^{(i)} + \omega_{\rm UV}]}$. The peak of the photoelectron spectrum at $\sqrt{2[-I_{\rm p}^{(i)} + \omega_{\rm UV}]}$ splits to $\sqrt{2[\pm\frac{\Omega}{2} - I_{\rm p}^{(i)} + \omega_{\rm UV}]}$. The width of peaks on the spectra is determined by $|b(p)\sigma| = 1/\sigma$, which is described in Eq. (4) in the absence of THz field as $\alpha = 0$. We can observe that a rising σ (longer pulse) results in the reduced width of photoelectron peaks, leading to an increasing frequency resolution, whereas the increasing α, proportional to the field strength of THz, will broaden the photoelectron peaks.

Taking a two-level system as an example, Rabi oscillation can be directly observed with the ultrashort pulse on photoelectron spectra.[25,26] However, the real-time observation of Rabi oscillation depends on the pulse width of the laser field as presented in Fig. 1, in which the width of probe pulse should be short enough. We take the energy levels of $5S_{\frac{1}{2}}$ ($|g\rangle$) and $5P_{\frac{3}{2}}$ ($|e\rangle$) in the rubidium atom as the ground state and the excited state, respectively. The intensity of the pump field is 0.013 a.u. (6×10^{12} W/cm^2) and the frequency of the pump pulse is 0.058 a.u., resonant with the transition between $5S_{\frac{1}{2}}$ and $5P_{\frac{3}{2}}$, as shown in Fig. 1(a). The ionization potentials of states $5S_{\frac{1}{2}}$ and $5P_{\frac{3}{2}}$ are $I_{\rm p}^{(\rm g)} = 0.154$ a.u. (4.18 eV) and $I_{\rm p}^{(\rm e)} = 0.096$ a.u. (2.59 eV), respectively. The UV probe laser with the wavelength of 266 nm (0.1713 a.u. and 4.64 eV) and the peak field amplitude of 0.005 a.u. (intensity $\sim 9 \times 10^{11}$ W/cm^2) is applied. The spectral peaks are located at $p_{\rm gg} = 0.186$ a.u. (red dotted line) and $p_{\rm ee} = 0.388$ a.u. (green dotted line) ionized from states $5S_{\frac{1}{2}}$ and $5P_{\frac{3}{2}}$, respectively. The electrons are initially prepared in $5S_{\frac{1}{2}}$. Rabi oscillation is prepared to occur at $\tau = 97.5$ fs by switching on the pump field. We present the dependence of the photoelectron momentum spectra with various pulse widths in Figs. 1(b)–1(d). When the probe pulse width is short as 4.8 fs in the FWHM, Rabi oscillations of 11.76 fs can be clearly distinguished. It is shown that Rabi oscillations are getting vague for the probe pulse duration of 9.7 fs and almost undetectable for 14.6 fs, as shown Figs. 1(c) and 1(d), respectively. In contrast, due to the time-frequency uncertainty principle with the probe pulse, one notes that ATSs on the photoelectron momentum spectrum with 14.6 fs pulse duration in Fig. 1(d) appear to be benefited with better frequency resolution, whereas they cannot be observed for 4.8 fs pulse duration in Fig. 1(b).

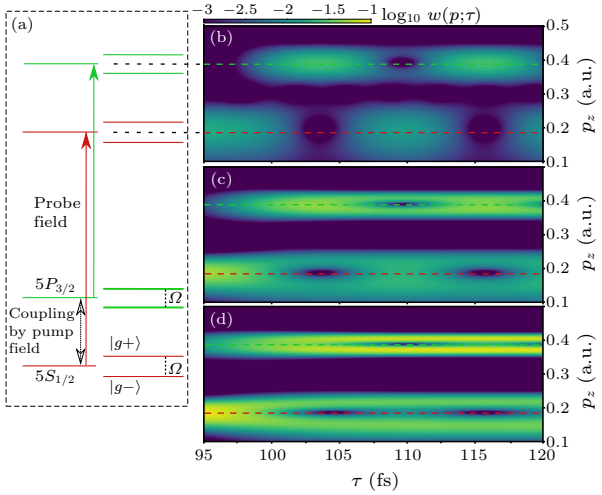

Fig. 1. The schematic of energy levels, and ATSs and Rabi oscillations in photoelectron momentum distribution at different probe-pulse durations. Panel (a) shows a two-level system, in which the Rabi oscillation thereon is driven by a resonant pump pulse and electrons are ionized by an UV pulse of 266 nm. The momentum distributions $w(p;\tau)$ versus delay time τ for FWHMs of 4.8 fs, 9.7 fs and 14.6 fs in the probe pulse are shown in (b), (c) and (d), respectively. Populations are mapped into spectral peaks of different longitudinal momenta p in each panel.

The existence of the time-frequency uncertainty principle for the probe pulse allows to select high resolution either in frequency domain or in time domain, as discussed above. Here, we demonstrate the THz streaking-assisted method to enhance temporal resolution maintaining the same frequency resolution. Assuming that the same setup of pump field is used as in Fig. 1, we switch on and off the pump field at different instants to simulate an arbitrary control sequence. Rabi oscillation is prepared to start at 97.5 fs and end at 122 fs. The probe pulse with the wavelength of 266 nm and pulse duration of 24 fs is locked at the zero crossing of the 5.3 THz vector potential as shown in Fig. 2(a). The central frequency of the single-cycle THz pulse is 5.3 THz and the electric field

is 7.2×10^{-5} a.u. Scanning the probing fields over τ yields $w(p;\tau)$ as shown in Fig. 2. Figures 2(b) and 2(c) show the spectrograms before and after applying the streaking THz field, respectively. The spectral peaks located at $p_{\rm gg}$ and $p_{\rm ee}$ split as Rabi oscillation is prepared to occur at $\tau = 97.5$ fs, and merge into one peak after switching off the pump field at $\tau = 122$ fs. With the THz field assisted, two pairs of ATSs in Fig. 2(c) are significantly broadened and fringes appear. These fringes can be assigned to be quantum coherence of ATSs. Meanwhile, they also reflect population evolution of the ground state $5S_{\frac{1}{2}}$ and the excited state $5P_{\frac{3}{2}}$.

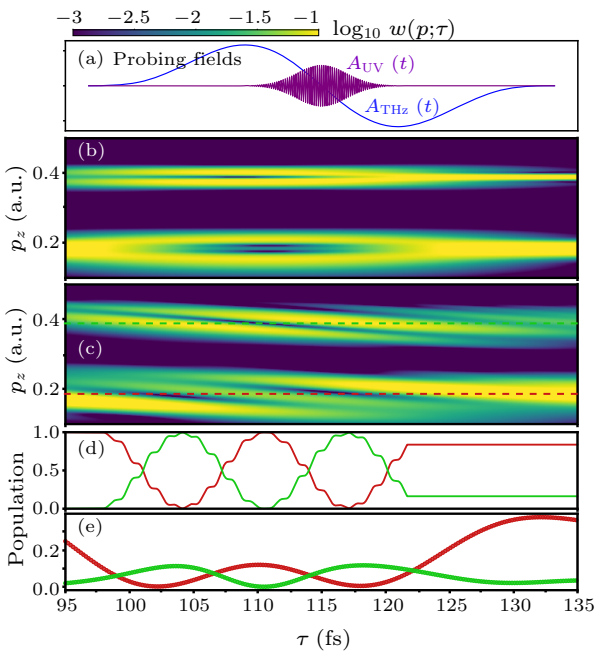

Fig. 2. The configuration of the probe pulse synchronized with THz field and THz SAPS for ATSs and Rabi oscillation. The 266 nm laser pulse (in purple) is well synchronized with a THz streaking pulse (in blue) in panel (a). The momentum distributions $w(p;\tau)$ with the probe pulse duration of 24 fs as a function of delay time τ are shown in panel (b) without THz streaking field and in panel (c) with THz streaking field, respectively. The calculated $w(p;\tau)$ and the projections along the momenta $p_{\rm gg}$ and $p_{\rm ee}$ in panel(c) are plotted in panel (e), where population evolution in the ground state and the excited state are indicated in red line and in green line, respectively.

Quantum coherences of ATSs along $p_{\rm gg}$ and $p_{\rm ee}$ in Fig. 2(c) are determined by the real part of $W_{\rm coh}(p;\tau)$ in Eq. (5), in which fringes with certain frequency appear. Correspondingly, population evolutions of the ground state and the excited state, displaying a Rabi oscillation period of 11.76 fs, are calculated by solving the equation for a laser-dressed two-level system, plotted in blue line and in red line in Fig. 2(d), respectively. The projections extracted along the momentum $p_{\rm gg}$ (red line) and $p_{\rm ee}$ (green line) in Fig. 2(c) are plotted in Fig. 2(e), which presents population evolutions synchronous with that in Fig. 2(d). The extracted oscillation period of about 13 fs is also consistent with the theoretical value. The switch-off time of pump pulse can be used to control final populations of the ground state and the excited state.

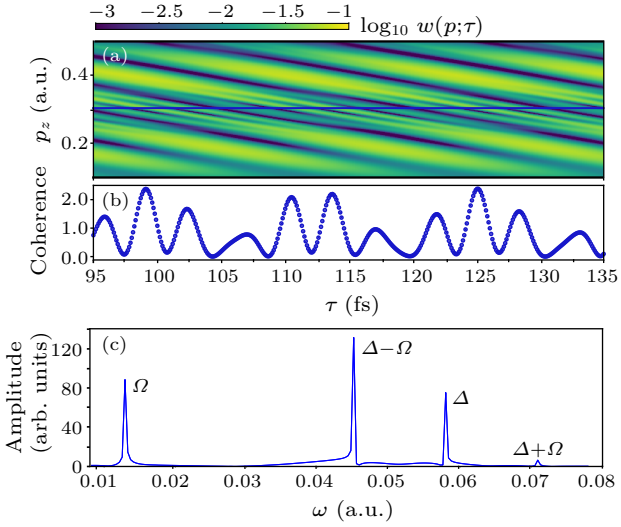

Fig. 3. THz SAPS and the frequency spectrum. The panel (a) is the same as the panel (c) in Fig. 3 but with higher THz intensity (1.5×10^{-4} a.u.). The fringes for quantum coherence are observed along $p_{\rm ge}$ which is indicated in blue line in panel (a) are projected in panel (b). The frequency spectrum extracted with Fourier transform of that in panel (b) is given in panel (c).

As the field strength of THz rises, the coherence between $5S$ and $5P$ states can be studied. When the THz field is sufficiently high, $|b(p)\sigma|^2$ becomes large and leads to the significantly broadened Gaussian peak, and all components in Eq. (3) contribute to the formation of spectral features at the characteristic momentum $p_{\rm ge} = \sqrt{2[\omega_{266} - [I_{\rm p}^{\rm (g)} + I_{\rm p}^{\rm (e)}]/2]} = 0.304$ a.u. Increasing the THz field from 7.2×10^{-5} a.u. to 1.5×10^{-4} a.u., we recalculate dynamics $w(p;\tau)$ of the system at the momentum p and the time τ in Fig. 3(a). It is seen that our calculations give the same ATS fringes as shown in Fig. 2(c) at $p_{\rm gg}$ and $p_{\rm ee}$, whereas there are more complicated structures in between. The coherence fringes described by the real part of $W_{\rm coh}(p;\tau)$ as shown in Eq. (5) are extracted along the momentum $p_{\rm ge}$ shown by the blue line in Fig. 3(a), which is displayed in Fig. 3(b). The corresponding frequency spectrum with Fourier transform is shown in Fig. 3(c), where four frequencies are present. The first peak and the third peak located at about 0.013 a.u. (11.8 fs) and 0.058 a.u. (2.62 fs), respectively, are in good agreement with the theoretical Rabi frequency and quantum beat $\Delta = I_p^{\rm (g)} - I_p^{\rm (e)}$ between $5S$ and $5P$ states. The second peak and the fourth peak correspond to combinations $\Delta + \Omega = 0.071$ a.u. and $\Delta - \Omega = 0.046$ a.u. of two frequencies, respectively.

The spectral peak in between contains all frequency components of possible Δ_{ij} between energies $E \in \{E_{\rm g} - \frac{\Omega}{2}, E_{\rm g} + \frac{\Omega}{2}, E_{\rm e} - \frac{\Omega}{2}, E_{\rm e} + \frac{\Omega}{2}\}$, that is, $\Delta_{ij} \in \{\Delta, \Omega, \Delta - \Omega, \Delta + \Omega\}$. Frequency components $\Delta - \Omega$ and $\Delta + \Omega$ originate from coherences of $\rho_{\rm g+,e-}$ and $\rho_{\rm g-,e+}$, respectively, with spec-

tral coefficients $W_{\rm coh} = 2e^{-\frac{(\Delta-\Omega)^2}{4|b(p)\sigma|^2}}{\rm Re}[\rho_{\rm g+,e-}]$ and $2e^{-\frac{(\Delta+\Omega)^2}{4|b(p)\sigma|^2}}{\rm Re}[\rho_{\rm g-,e+}]$. Both the partial spectral peaks share the same center at $p_{\rm ge}$. The coefficient for $\rho_{\rm g+,e-}$ is larger than that of $\rho_{\rm g-,e+}$ as presented in Fig. 3(c). Another spectral component Δ comes from the contributions of $\rho_{\rm g+,e+}$ and $\rho_{\rm g-,e-}$. The centers of associated spectral peaks are close to $p_{\rm ge}$, though they are not exactly localized. With Eq. (3), both coefficients are proportional to $2\exp[-(\Delta^2+\Omega^2)/4|b(p)\sigma|^2]$. On the other hand, the spectral component Ω results from the contributions of $\rho_{\rm g+,g-}$ and $\rho_{e+,e-}$. Even though the centers of their spectral peaks are far away from $p_{\rm ge}$, factor $\exp[-(\Delta_{ij}/2)^2/|b(p)\sigma|^2]$ in Eq. (3) is much larger than that of Δ. In fact, Eq. (3) shows that the coefficient for component Ω is identical to the one for Δ, which is also proportional to $2\exp[-(\Delta^2+\Omega^2)/4|b(p)\sigma|^2]$, thus their spectral components is comparable. With all their coefficients evaluated and note that the factors have $(\Delta+\Omega)^2 > \Delta^2+\Omega^2 > (\Delta-\Omega)^2$, the spectral distribution in Fig. 3 simply verifies the contributions from coherences.

For the two-level system of the rubidium atom, the probe pulse of 24 fs synchronized with a THz field enable us to well visualize Rabi oscillation of ∼11.76 fs. Meanwhile, quantum beat of ∼2.6 fs between the states of $5S_{\frac{1}{2}}$ and $5P_{\frac{3}{2}}$ is also visible clearly, whose time scale is almost ten times shorter than the probe-pulse duration. Therefore, the THz SAPS is found to be an effective method for direct observations of ultrafast coherence dynamics with temporal resolution beyond the pulse duration. In addition, the use of long probe pulse itself maintains sufficiently high frequency resolution in photoelectron spectroscopy, which allows to observe Autler–Townes splittings. Such proposed experiments are feasible in the wake of development of Rb magneto-optical trap recoil ion momentum spectroscopy.[27−29]

In summary, by employing THz SAPS to study Rabi oscillation and population evolution, we show a potential application for time-resolved measurements of ultrafast coherence dynamics with significantly enhanced time resolution. The UV pulse induces the single-photon ionization, liberating the electron of the superposed state. The THz wave kinetically rearranges electronic trajectories and creates the interference between trajectories from different initial states at the final momentum distribution $w(p;\tau)$. The temporal evolution of the system at τ can be mapped directly onto $w(p;\tau)$. The coherence and population dynamics between the states can be retrieved from the fringes on $w(p;\tau)$, less restricted by the duration of probing pulse than in conventional transient spectroscopies, showing the potential applicability to study and control ultrafast coherence dynamics on a tabletop-scale experimental platform.

References

[1] Brinks D, Hildner R, Van Dijk E M, Stefani F D, Nieder J B, Hernando J and Van Hulst N F 2014 *Chem. Soc. Rev.* **43** 2476
[2] Krausz F and Ivanov M 2009 *Rev. Mod. Phys.* **81** 163
[3] Gallmann L, Cirelli C and Keller U 2012 *Annu. Rev. Phys. Chem.* **63** 447
[4] Nisoli M, Decleva P, Calegari F, Palacios A and Martín F 2017 *Chem. Rev.* **117** 10760
[5] Tamai N and Miyasaka H 2000 *Chem. Rev.* **100** 1875
[6] Zewail A H 2000 *J. Phys. Chem. A* **104** 5660
[7] Bergmann K, Theuer H and Shore B W 1998 *Rev. Mod. Phys.* **70** 1003
[8] Goulielmakis E, Loh Z H, Wirth A, Santra R, Rohringer N, Yakovlev V S, Zherebtsov S, Pfeifer T, Azzeer A M, Kling M F and Leone S R 2010 *Nature* **466** 739
[9] Senftleben A, Hemmer M, Schröter C D, Ullrich J, Pfeifer T and Moshammer R 2016 *Science* **354** 308
[10] Rabi I I 1937 *Phys. Rev.* **51** 652
[11] Autler S H and Townes C H 1955 *Phys. Rev.* **100** 703
[12] Saffman M, Walker T G and Mølmer K 2010 *Rev. Mod. Phys.* **82** 2313
[13] Saglamyurek E, Hrushevskyi T, Rastogi A, Heshami K and LeBlanc L J 2018 *Nat. Photon.* **12** 774
[14] Girju M G, Hristov K, Kidun O and Bauer D 2007 *J. Phys. B* **40** 4165
[15] Sun Z and Lou N 2003 *Phys. Rev. Lett.* **91** 023002
[16] Fushitani M, Liu C N, Matsuda A, Endo T, Toida Y, Nagasono M, Togashi T, Yabashi M, Ishikawa T, Hikosaka Y and Morishita T 2016 *Nat. Photon.* **10** 102
[17] Itatani J, Quéré F, Yudin G L, Ivanov M Y, Krausz F and Corkum P B 2002 *Phys. Rev. Lett.* **88** 173903
[18] Goulielmakis E, Uiberacker M, Kienberger R, Baltuska A, Yakovlev V, Scrinzi A, Westerwalbesloh T, Kleineberg U, Heinzmann U, Drescher M and Krausz F 2004 *Science* **305** 1267
[19] Gaumnitz T, Jain A, Pertot Y, Huppert M, Jordan I, Ardana-Lamas F and Wörner H J 2017 *Opt. Express* **25** 27506
[20] Gagnon J and Yakovlev V S 2009 *Opt. Express* **17** 17678
[21] P, Doumy G, Roedig C, Gagnon J, Messerschmidt M, Schorb S and Bostedt C 2014 *Nat. Photon.* **8** 950
[22] Kowalewski M, Bennett K, Rouxel J R and Mukamel S 2016 *Phys. Rev. Lett.* **117** 043201
[23] Lindenblatt H, Trost F, Liu Y, Stojanovic N, Al-Shemmary A, Golz T and Treusch R 2019 *Phys. Rev. Lett.* **122** 073001
[24] Zhang Y, Yan T M and Jiang Y H 2018 *Phys. Rev. Lett.* **121** 113201
[25] Vasa P, Wang W, Pomraenke R, Lammers M, Maiuri M, Manzoni C, Cerullo G and Lienau C 2013 *Nat. Photon.* **7** 128
[26] Johnson T A, Urban E, Henage T, Isenhower L, Yavuz D D, Walker T G and Saffman M 2008 *Phys. Rev. Lett.* **100** 113003
[27] Li R, Yuan J, Wang X, Hou X, Zhang S, Zhu Z, Ma Y, Gao Q, Wang Z, Yan T M and Qin C 2019 *J. Instrum.* **14** P02022
[28] Yuan J, Ma Y, Li R, Ma H, Zhang Y, Ye D, Shen Z, Yan T, Wang X, Weidemüller M and Jiang Y 2020 *Chin. Phys. Lett.* **37** 053201
[29] Yuan J, Liu S, Wang X, Shen Z, Ma Y, Ma H, Meng Q, Yan T, Zhang Y, Dorn A, Weidemüller M, Ye D and Jiang Y 2020 *Phys. Rev. A* **102** 043112